Q. J. R. Meteorol. Soc. (2002), **128**, pp. 1689–1712

A study on the optimization of the deployment of targeted observations using adjoint-based methods

By THIERRY BERGOT* and ALEX DOERENBECHER
Météo-France, France

(Received 18 June 2001; revised 29 October 2001)

SUMMARY

A new adjoint-based method to find the optimal deployment of targeted observations, called Kalman Filter Sensitivity (KFS), is introduced. The major advantage of this adjoint-based method is that it allows direct computation of the reduction of the forecast-score error variance that would result from future deployment of targeted observations. This method is applied in a very simple one-dimensional context, and is then compared to other adjoint-based products, such as classical gradients and gradients with respect to observations. The major conclusion is that the deployment of targeted observation is strongly constrained by the aspect ratio between the length-scale of the sensitivity area and the length-scale of the analysis-error covariance matrix. This very simple example also clearly illustrates that the reduction of forecast-error variance is stronger for assimilation schemes which have a smaller characteristic length-scale. Finally, the KFS technique is applied in a diagnostic way (i.e. once the observations are done) to four FASTEX cases. For these cases, the reduction of the forecast-error variance is in agreement with the efficiency of targeted observations as previously studied. A preliminary step towards an operational use has been performed on FASTEX IOP18, and results seem to validate the KFS approach of targeting.

KEYWORDS: Adjoint methods Kalman filter Predictability

1. INTRODUCTION

The forecast of some meteorological events (like rapid cyclogenesis) remains a difficult problem, even at short range (typically 12–48 h). These situations are often very problematic for the forecasters and can, moreover, have a dramatic socio-economical impact. Even if the model can simulate the evolution of the atmosphere perfectly, errors in the initial conditions may amplify rapidly and degrade the forecasts. These errors in the initial conditions are a consequence either of the errors in the observations, or of the inhomogeneous observational network (areas with insufficient or inaccurate observations), or of the assimilation scheme which transforms the observations into model initial conditions.

In order to try to improve the forecasting of such events, a new observational strategy, called adaptive or targeted, has been proposed. The principle is to add an adaptive component to the conventional network of observations. Adaptive observations are intended to reduce the forecast-error variance of a forecast with a high potential socio-economic impact. It is adaptive in the sense that the locations of these measurements vary from day to day. The problem is then to locate the targeted observations, in an optimal way (in the sense of lowest cost or minimum number of observations versus maximum improvement of the forecast). The forecast errors, in a perfect model context, are a consequence either of errors in the initial conditions, or of initial-error growth. During the past years, several solutions have been suggested for finding the optimal locations of adaptive observations and thus to define targeting strategies, and these strategies have been tested during the Fronts and Atlantic Storm-Track EXperiment (FASTEX) field experiment (Emanuel and Langland 1998; Joly *et al.* 1999), the North Pacific Experiment field experiment (Langland *et al.* 1999a) and the US Winter Storm Reconnaissance program (Szunyogh *et al.* 2000).

* Corresponding author: Météo-France, CNRM/GMME, 42 avenue G. Coriolis, F-31057 Toulouse Cedex, France.
e-mail: Thierry.Bergot@meteo.fr

The first method is based on an estimation of the uncertainty in the analyses and on an estimation of the time evolution of this uncertainty with an ensemble of forecasts (ensemble transform technique, Bishop and Toth 1999). The main goal is to find the location of observations that will minimize a given norm of the forecast-error variance inside a verifying area. This method combines both the statistical distribution of the errors and error growth (represented by the evolution of the ensemble of forecasts). However, this technique does not take into account the fact that observations have to go through the data assimilation processes to produce initial conditions. Moreover, the efficiency of targeted observations strongly depends on the assimilation scheme (Morss 1999; Bergot 2001). A new method, called Ensemble Transform Kalman Filter (ETKF), has been recently proposed by Bishop *et al.* (2001), and has been used during the Winter Storm Reconnaissance Program 2000 and 2001. Majumdar *et al.* (2001) have tested the ability of the ETKF to quantitatively estimate the reduction in the forecast-error variance with the National Centers for Environmental Prediction (NCEP) operational forecast model.

The second method focuses on initial-error growth and is based on adjoint products (Palmer *et al.* 1998; Bergot *et al.* 1999; Gelaro *et al.* 1999; Langland *et al.* 1999b). This method relies on the fact that the initial errors in an unstable subspace of small dimension play a key role in the forecast errors. If small errors exist in these unstable directions, they will rapidly grow and degrade the forecast. The idea is then to concentrate observations inside the sensitive area, in order to minimize the initial error. To take the assimilation processes into account, the sensitivity to observations has been constructed (Baker and Daley 2000; Doerenbecher and Bergot 2001). However, these sensitivity fields do not indicate where initial errors are, they only suggest where observations may have a big effect on the forecast. These adjoint-based strategies include only a little information about the probable location of the initial errors. Moreover, some studies have shown that it is important to take into account the statistical distribution of the errors, even if the dynamical processes prevail in the forecast-error growth (Lorenz and Emanuel 1998; Morss *et al.* 2001).

To take this fact into account, a new simple method, based on sensitivity and called Kalman Filter Sensitivity (KFS), is proposed. Also tested in a simple context is how this method can take into account the assimilation process, the expected quality of the analysed field, and the way these uncertainties can be propagated by the atmospheric dynamics (sections 3 and 4). And finally, this method will be illustrated in FASTEX cases (section 5).

2. Formulation of the problem

The sensitivity of one aspect of the forecast to initial conditions has been the subject of many studies during the past years (Rabier *et al.* 1996; Errico 1997). The classical framework of these studies was to determine the variation of a forecast aspect J as a function of the modification of the initial conditions $\mathbf{x}_a(t0)$. However, the sensitivity fields do not indicate the likely location of initial errors, they only suggest where to look for initial conditions that may have a big effect on the forecast. The impact of observations on the forecast is the combination of the sensitivity and the initial errors, and the observations that give the maximum impact are not necessarily located in the area with the highest sensitivities (Doerenbecher and Bergot 2001). Since one cannot determine the amplitude of the initial error before the observations are done, and since analysis errors partly arise from unknown errors in the measurements, it seems natural to include the statistical distribution of the analysis errors in an operational targeting

context. Berliner *et al.* (1999) have formulated the targeted-observations problem in a rigorous statistical framework. However, the proposed optimization is virtually intractable in very high-dimensional problems, such as an operational numerical weather forecast model. The aim of this section is to describe a simplified method, based on sensitivity fields, on statistical distribution of the errors, and on the assimilation scheme.

(*a*) *Estimation of the variance of a forecast score*

In the adaptive observation problem, it is crucial to provide an estimate of the reduction of the forecast-error variance due to the inclusion of targeted observations. An approach, in theoretical study, to evaluate this forecast-error variance is to use a Kalman filter, and to try to minimize some components of these forecast-error variances (for example, the sum of the forecast-error variance at different points of interest). However, a key difficulty is that the computation of such a criterion is impossible in current numerical weather prediction models, and numerical simplification and/or dimension reduction have to be performed.

Let $\mathbf{x}_{\text{true}}(t)$ be the true state of the atmosphere at time t, and let $\mathbf{x}_{\text{a}}(t)$ be the state vector at time t resulting from the assimilation process, and $\mathbf{x}_{\text{f}}(t)$ a forecast at time t. Let $t0$ be the initialization time and $t1$ be the final, or verification, time at which a forecast aspect J was computed. Let us define a forecast score S, depending on J:

$$S = J(\mathbf{x}_{\text{f}}(t1)) - J(\mathbf{x}_{\text{true}}(t1)). \tag{1}$$

It is proposed to compute the variance of the forecast score S. This variance gives us an estimate of the predictability of J at time $t1$, and is given by

$$(\sigma_S)^2 = \overline{\{J(\mathbf{x}_{\text{f}}(t1)) - J(\mathbf{x}_{\text{true}}(t1))\}^2} - \overline{J(\mathbf{x}_{\text{f}}(t1)) - J(\mathbf{x}_{\text{true}}(t1))}^2. \tag{2}$$

The first step is to evaluate the second term of Eq. (2) and therefore to calculate the bias of S at time $t1$. This bias is given by

$$\overline{S} = \overline{J(\mathbf{x}_{\text{f}}(t1)) - J(\mathbf{x}_{\text{true}}(t1))}. \tag{3}$$

Following the first-order expansion of J, the bias is estimated under the linear hypothesis by

$$\overline{S} \simeq \overline{(\mathrm{d}J/\mathrm{d}\mathbf{x}(t1))^{\mathrm{T}} \cdot (\mathbf{x}_{\text{f}}(t1) - \mathbf{x}_{\text{true}}(t1))}. \tag{4}$$

If the forecast model $\mathcal{M}$ is perfect, then $\mathbf{x}_{\text{true}}(t1) = \mathcal{M}\mathbf{x}_{\text{true}}(t0)$. Let $\mathbf{M}$ be the linear approximation or tangent linear model of the forecast model $\mathcal{M}$, and $\mathbf{M}^{\mathrm{T}}$ the adjoint model. Then, the first-order approximation of the bias of S is given by

$$\overline{S} \simeq \overline{(\mathbf{M}^{\mathrm{T}}\,\mathrm{d}J/\mathrm{d}\mathbf{x}(t1))^{\mathrm{T}} \cdot (\mathbf{x}_{\text{a}}(t0) - \mathbf{x}_{\text{true}}(t0))}. \tag{5}$$

Following the classical notations of sensitivity studies, one notes the sensitivity field $\nabla_{\mathbf{x}} J = \mathbf{M}^{\mathrm{T}}\,\mathrm{d}J/\mathrm{d}\mathbf{x}(t1)$. The adjoint model is based on a trajectory, issued from a nonlinear run. As long as the change to this trajectory evolves nearly linearly between $t0$ and $t1$, the gradient field remains basically unchanged (Harrison *et al.* 1999; Baker 2000). Consequently, $\mathbf{M}^{\mathrm{T}}\,\mathrm{d}J/\mathrm{d}\mathbf{x}(t1)$ would not change substantially, and the assumption that

$$\overline{\mathbf{M}^{\mathrm{T}}\,\mathrm{d}J/\mathrm{d}\mathbf{x}(t1)} = \mathbf{M}^{\mathrm{T}}\,\mathrm{d}J/\mathrm{d}\mathbf{x}(t1)$$

seems reasonable. Under this hypothesis, the bias $\overline{S}$ at time $t1$ may be written in the form

$$\overline{S} \simeq (\nabla_{\mathbf{x}} J)^{\mathrm{T}} \cdot \overline{(\mathbf{x}_{\text{a}}(t0) - \mathbf{x}_{\text{true}}(t0))}. \tag{6}$$

Given the fact that the analysis is an unbiased process, $\overline{(\mathbf{x}_a(t0) - \mathbf{x}_{true}(t0))} = 0$, and consequently the statistical distribution of S is non-biased:

$$\overline{S} = 0. \tag{7}$$

Given Eq. (7), the second term of Eq. (2) is zero, and following the previous notations and hypotheses, the variance of S at time $t1$ can be written in the form

$$(\sigma_S)^2 = \overline{\{(\nabla_{\mathbf{x}} J)^{\mathrm{T}} \cdot (\mathbf{x}_a(t0) - \mathbf{x}_{true}(t0))\}^2}. \tag{8}$$

This expression can be developed into

$$(\sigma_S)^2 = (\nabla_{\mathbf{x}} J)^{\mathrm{T}} \cdot \overline{(\mathbf{x}_a(t0) - \mathbf{x}_{true}(t0))(\mathbf{x}_a(t0) - \mathbf{x}_{true}(t0))^{\mathrm{T}}} \cdot \nabla_{\mathbf{x}} J. \tag{9}$$

Using the mathematical definition of the analysis-error covariance matrix $\mathbf{A}$, the variance of the score at time $t1$ may be written in the generalized form (see also the demonstrations done in Baker (2000) and Bishop *et al.* (2001))

$$(\sigma_S)^2 = (\nabla_{\mathbf{x}} J)^{\mathrm{T}} \cdot \mathbf{A} \cdot \nabla_{\mathbf{x}} J. \tag{10}$$

Given the statistical distribution of the initial error (due to errors in the background field and errors in the observations), and the dynamical properties of the atmosphere (represented by the sensitivity field), one can easily determine the variance of a score S of one aspect J of the forecast at verification time.

(*b*) *Minimization of the variance of a forecast score*

In adaptive observations, one generally considers the observational network to be composed of a routine or conventional network (denoted by a subscript c) and an adaptive or targeted component (denoted by a subscript t). Let $\mathbf{A}_c$ (respectively, $\mathbf{A}_{c+t}$) be the analysis-error covariance matrix, given by the assimilation of conventional observations (respectively, conventional and targeted observations). Following Eq. (10), the variance of the score of the forecast at verification time $t1$ for the combined conventional and adaptive observations is given by

$$(\sigma_S^{c+t})^2 = (\nabla_{\mathbf{x}} J)^{\mathrm{T}} \cdot \mathbf{A}_{c+t} \cdot \nabla_{\mathbf{x}} J. \tag{11}$$

If the errors of the targeted observations are uncorrelated with errors in the conventional observations, the covariance matrix of analysis errors issued from the assimilation of both conventional and targeted networks is given by

$$\mathbf{A}_{c+t} = (\mathbf{B}^{-1} + \mathbf{H}_c^{\mathrm{T}} \mathbf{R}_c^{-1} \mathbf{H}_c + \mathbf{H}_t^{\mathrm{T}} \mathbf{R}_t^{-1} \mathbf{H}_t)^{-1}, \tag{12}$$

where $\mathbf{B}$ and $\mathbf{R}$ are the background-error covariance matrix and the observation-error covariance matrix, respectively; $\mathbf{H}$ is the linear observation operator, which interpolates from model to the observation space; note that we suppose here that these matrices are accurately specified.

Using the Sherman–Morrison–Woodbury formula, one may rewrite $\mathbf{A}_{c+t}$ as a function of the statistical characteristic of both conventional and targeted observations:

$$\mathbf{A}_{c+t} = \mathbf{A}_c - \mathbf{A}_c \mathbf{H}_t^{\mathrm{T}} (\mathbf{R}_t + \mathbf{H}_t \mathbf{A}_c \mathbf{H}_t^{\mathrm{T}})^{-1} \mathbf{H}_t \mathbf{A}_c. \tag{13}$$

Substituting Eq. (13) in Eq. (11), one can decompose the variance of the score into two terms: the first one concerns the effect of the conventional network of observations, and the second term represents the effect of the targeted observations, given the conventional

observations and the assimilation scheme

$$
\begin{aligned}
(\sigma_S^{c+t})^2 &= (\nabla_{\mathbf{x}} J)^{\mathrm{T}} \cdot \mathbf{A}_{c+t} \cdot \nabla_{\mathbf{x}} J \\
&= (\nabla_{\mathbf{x}} J)^{\mathrm{T}} \cdot \{\mathbf{A}_c - \mathbf{A}_c \mathbf{H}_t^{\mathrm{T}} (\mathbf{R}_t + \mathbf{H}_t \mathbf{A}_c \mathbf{H}_t^{\mathrm{T}})^{-1} \mathbf{H}_t \mathbf{A}_c\} \cdot \nabla_{\mathbf{x}} J \\
&= (\sigma_S^c)^2 - (\nabla_{\mathbf{x}} J)^{\mathrm{T}} \cdot \mathbf{A}_c \mathbf{H}_t^{\mathrm{T}} (\mathbf{R}_t + \mathbf{H}_t \mathbf{A}_c \mathbf{H}_t^{\mathrm{T}})^{-1} \mathbf{H}_t \mathbf{A}_c \cdot \nabla_{\mathbf{x}} J. \qquad (14)
\end{aligned}
$$

Therefore, the reduction in the variance of the score, due to the inclusion of the targeted observations, is given by

$$
(\delta\sigma_S^t)^2 = (\nabla_{\mathbf{x}} J)^{\mathrm{T}} \cdot \mathbf{A}_c \mathbf{H}_t^{\mathrm{T}} (\mathbf{R}_t + \mathbf{H}_t \mathbf{A}_c \mathbf{H}_t^{\mathrm{T}})^{-1} \mathbf{H}_t \mathbf{A}_c \cdot \nabla_{\mathbf{x}} J. \qquad (15)
$$

This expression allows a quantitative prediction of the reduction of the forecast-error variance in the unstable direction of the sensitivity field to be made, provided that the error covariances are accurately specified and that the errors evolve linearly. Inaccuracies in error covariances that are specified by the assimilation scheme can lead to errors in the estimations of the forecast-score variance. However, this remark is valid for all studies which aim at estimating the forecast-error variance (see also Majumdar *et al.* 2001). One hopes that substantial effort will be made in the near future to improve estimates of the background-error covariances, and therefore to increase the relevance of this kind of study. It should also be noted that Eq. (15) focuses on the variance of the forecast error in the direction given by the sensitivity. Therefore, as for studies based on sensitivity fields, one focuses on one given aspect of the forecast, J. The goal is to reduce the variance of the score given by this forecast aspect. This kind of approach is in agreement with the targeted observation concept: when a meteorological event with a possible high socio-economic impact is forecast, the forecaster defines the forecast aspect associated with this socio-economic impact (strong wind, rainfall, and so on), and Eq. (15) gives the location of adaptive observations that allow the variance of the error on the selected forecast aspect to be reduced.

To optimize the location of targeted observations (in a statistical sense), it is necessary to obtain a maximum decrease of the variance of the forecast score. The problem is to find $\mathbf{H}_t$, given the statistical characteristics of the conventional network, that maximizes Eq. (15). This is a matricial optimization problem, which involves complicated mathematical techniques (so-called linear optimization design, see Fedorov *et al.* (1972)) such as the Simplex method, to be solved in an optimal way. Note that this problem can be solved before any observations are performed, since only the statistical characteristics of the observations and of the background field are needed. Although the location of some conventional observations (such as the cloud-track wind vectors, for example) are difficult to predict accurately, one assumes for the sake of simplicity that the state of the conventional observations is exactly known.

The first difficulty lies in the estimation of the analysis-error covariance matrix $\mathbf{A}_c$. Most of the current assimilation schemes use the variational method in which the analysis state is defined as a minimum of a cost function. This means that the analysis-error covariance matrix is not computed during the minimization. However, several methods exist for getting an estimate of it (Fisher and Courtier 1995). It should be noted that Eq. (15) depends on the covariance error matrices $\mathbf{A}_c$ and $\mathbf{R}_t$. If these matrices are inaccurately specified, the optimal location of targeted data could be inaccurate as well. It seems particularly essential to get a precise estimate of $\mathbf{A}_c$ in the direction of the sensitivity $\nabla_{\mathbf{x}} J$. Following the work of Fisher and Courtier (1995), Doerenbecher and Bergot (2001) showed how it is possible with the Lanczos algorithm to obtain an accurate estimate of $\mathbf{A}_c$ in the unstable direction of the sensitivity, in an operational assimilation context.

The second difficulty for the computation of Eq. (15) lies in the estimation of the inverse of the so-called 'innovation of targeted covariance matrix' $\mathbf{R}_t + \mathbf{H}_t\mathbf{A}_c\mathbf{H}_t^T$. The size of this matrix is the number of the targeted observations, N_t. For currently operational targeted applications (such as the definition of an optimal flight plan), $N_t \ll 1000$, and this matrix could be directly inverted. Another possibility for solving the problem practically is to find the optimal location of the targeted observations in a sequential manner, as explained in Bishop *et al.* (2001). In this case, one wants to find a sub-optimal solution of the problem by first identifying the best location of a single targeted observation. Once this location has been found, one can find the location of the second targeted observation, taking into account the effect of the previous targeted observation. This sequential method is very efficient for simplifying the problem; however, it is only a sub-optimal method, in opposition to the solution given by the global optimization of Eq. (15). In the case of such a method, the size of the innovation covariance matrix is reduced to the size of one targeted observation, which makes its inversion even easier.

The proposed method given by Eq. (15) can be seen as a simplified evaluation of the reduction of the forecast-error covariance in the direction of the sensitivity field. Following Eq. (10), and the fact that $\nabla_{\mathbf{x}} J = \mathbf{M}^T \, \mathrm{d}J/\mathrm{d}\mathbf{x}(t1)$, the variance of the forecast score S is given by

$$\begin{aligned}(\sigma_S)^2 &= (\mathbf{M}^T \, \mathrm{d}J/\mathrm{d}\mathbf{x}(t1))^T \cdot \mathbf{A} \cdot (\mathbf{M}^T \, \mathrm{d}J/\mathrm{d}\mathbf{x}(t1)) \\ &= (\mathrm{d}J/\mathrm{d}\mathbf{x}(t1))^T \mathbf{M}\mathbf{A}\mathbf{M}^T \, \mathrm{d}J/\mathrm{d}\mathbf{x}(t1). \end{aligned} \tag{16}$$

The evolution of the forecast-error statistic $\mathbf{P}$ in a perfect model context is given by the Kalman filter theory:

$$\mathbf{P} = \mathbf{M}\mathbf{A}\mathbf{M}^T. \tag{17}$$

The comparison of Eq. (16) and Eq. (17) clearly shows that the variance of S is the projection of the forecast-error covariance on the direction of the gradient field at time $t1$.

The reduction of the forecast-error variance implied by Eq. (17), due to the inclusion of targeted data to the conventional network of observations, can also be estimated following Eq. (13):

$$\mathbf{P}_c - \mathbf{P}_{c+t} = \mathbf{M}\mathbf{A}_c\mathbf{H}_t^T(\mathbf{R}_t + \mathbf{H}_t\mathbf{A}_c\mathbf{H}_t^T)^{-1}\mathbf{H}_t\mathbf{A}_c\mathbf{M}^T. \tag{18}$$

In the same manner, it can easily be seen that the reduction of the variance of the score given by Eq. (15) is just an estimation of the reduction of the total forecast-error variance in the direction of the sensitivity. In this sense, the proposed method will be called 'Kalman Filter Sensitivity' (KFS).

3. Single targeted observation case

(*a*) *Mathematical simplification*

As previously discussed, the optimal location of targeted observations could be resolved by a sequential assimilation of a single targeted observation. In this case, the optimal location of targeted data could be simplified into the search of the optimal location of a single targeted observation. The aim of this section is to provide physical interpretations of the proposed optimal sampling strategy.

Suppose that a single targeted observation is to be performed, and that this observation will measure a single element of the state vector $\mathbf{x}_a(t0)$. Then, $\mathbf{H}_t$ is a single

row vector whose elements are all zero except for one element equal to 1. In a grid-point model, the single observation is located at a grid point and the location of the '1' element in $\mathbf{H}_t$ corresponds to the location of this observation; let this location be denoted by i. In this case, the targeted observation-error covariance matrix $\mathbf{R}_t$ is reduced to a scalar, σ_o^2. Let the conventional analysis covariance matrix be denoted $\mathbf{A}_c = [a_{j,k}]$, and the sensitivity field be denoted $\nabla_{\mathbf{x}} J = [g_k]$. For a single observation at point i, Eq. (15) reduces to

$$(\delta\sigma_S^i)^2 = \left(\sum_k a_{i,k} g_k \right)^2 \Big/ (\sigma_o^2 + a_{i,i}). \tag{19}$$

The proposed optimal sampling problem is to find i that maximizes this expression. With some approximations, this equation provides some clues. The numerator corresponds to the product of the matrix of conventional-analysis covariances with the gradient field $\mathbf{A}_c \cdot \nabla_{\mathbf{x}} J$, projected at the targeted observation point i. This expression is weighted by the sum of the variance of the conventional analysis at the targeted-observation point and the targeted-observation variance error. Suppose that the targeted observation is of good quality (i.e. $\sigma_o^2 \ll a_{i,i}$). If the characteristic length-scales of the covariance analysis-error matrix is smaller than the characteristic length-scales of the sensitivity field (i.e. if $\mathbf{A}_c$ is almost diagonal in the sensitive area), Eq. (19) can be simplified to $(\delta\sigma_S^i)^2 = a_{i,i} g_i^2$. The optimal location of the targeted data (in the sense of a maximum reduction of the variance of the forecast score) is therefore the region of maximum sensitivity weighted by the variance of the conventional-analysis error at this point. If $\mathbf{A}_c$ is almost diagonal, and if the diagonal terms are almost uniform over the sensitive area, the optimal sampling is mostly constrained by the dynamics (reflected by the sensitivity field). In this case, the optimal targeted observation is located where the absolute value of sensitivity is maximum. Alternatively, if the sensitivity field varies little with respect to the length-scale of the conventional-analysis covariances, the sampling strategy is dominated by the statistical characteristics of the conventional-analysis errors, and the optimal targeted observation is located where the variance of the conventional-analysis error is maximum. Of course, in real situations the optimal sampling strategy combines both the dynamics and the analysis errors.

(*b*) *Comparison with sensitivity to observations*

Another way to optimize the location of targeted observations is to use the so-called sensitivity to observations. Baker and Daley (2000) and Doerenbecher and Bergot (2001) suggested that the sensitivity with respect to observations could be an efficient tool for defining the location of targeted observations. One of the major advantages is that the sensitivity to observations is significantly reduced in regions already sampled by existing observations. Another advantage is that this kind of sensitivity takes into account the way in which the observations will be assimilated. With the previous notation, the sensitivity to targeted observations, $\mathbf{y}_t$ is given by

$$\nabla_{\mathbf{y}_t} J = \mathbf{R}_t^{-1} \mathbf{H}_t \mathbf{A}_{c+t} \cdot \nabla_{\mathbf{x}} J. \tag{20}$$

The covariance analysis-error matrix $\mathbf{A}_{c+t}$ can be determined using Eq. (13). For a single targeted observation at point i, this matrix reduces to

$$\mathbf{A}_{c+t} = \{a_{j,k} - a_{i,j} a_{i,k} / (\sigma_o^2 + a_{i,i})\}_{j,k}. \tag{21}$$

And the sensitivity to the targeted observation at point i is expressed by

$$\nabla_{\mathbf{y}_t} J(i) = \sum_k a_{i,k} g_k / (\sigma_o^2 + a_{i,i}). \tag{22}$$

If $a_{i,i}$ is almost uniform over the sensitive area (i.e. if the length-scale of the variance of $\mathbf{A}_c$ in the sensitive area is long compared to the length-scale of the sensitivity field), the two methods (KFS and sensitivity to observations) lead to the same optimal location of the targeted observation. This optimal location is also given by the maximum of $\mathbf{A}_c \cdot \nabla_{\mathbf{x}} J$. The optimal location is the place where the sensitivity, weighted by the analysis-error covariance matrix, is maximum. This case can arise, for example, if the diagonal term in $\mathbf{B}$ is almost constant inside the sensitive area and if the conventional data are only available far away from the latter.

Alternatively, if $a_{i,i}$ strongly varies in the sensitive area, for example if the sensitive area is located close to a well-observed area, the two methods can give significantly different optimal locations. To illustrate this point, let us decompose the elements of the covariance error matrix $\mathbf{A}_c$ into $a_{i,k} = \sigma_a(i)\sigma_a(k)\varrho(i, k)$. The first two terms $\sigma_a(i)$ and $\sigma_a(k)$ represent the standard deviation of the analysis errors at point i and k, respectively, and the third term represents the normalized correlation between these two points. Let us also denote $I(i) = \sum_k \varrho_{i,k} g_k$. This term can be seen as the product of the sensitivity field by the structure functions associated with the assimilation processes. Using this notation, the sensitivity to observations (Eq. (22)) is given by

$$\nabla_{\mathbf{y}_t} J(i) = \sigma_a^2(i) I(i)/(\sigma_o^2 + \sigma_a^2(i)), \tag{23}$$

and the KFS method (Eq. (19)) can be written in the form

$$(\delta\sigma_S^i)^2 = \sigma_a^4(i) I^2(i)/(\sigma_o^2 + \sigma_a^2(i)). \tag{24}$$

It can be easily seen that $(\delta\sigma_S^i)^2 = (\sigma_a^2(i) + \sigma_o^2)(\nabla_{\mathbf{y}_t} J(i))^2$. In this sense, the KFS method takes into account the way the targeted observations will modify the initial conditions through the assimilation process, and the way these modifications could be propagated by the model. Moreover, it takes into account the quality of the conventional analysed field. It would be useful to recall here that Eqs. (23) and (24), and therefore this discussion, apply to a single observation only.

4. Application in a simple 1D framework

(*a*) *Simple 1D analysis framework*

In order to better understand the optimal sampling problem, a very simple one-dimensional (1D) univariate analysis system, quite similar to the one used by Baker and Daley (2000), has been constructed. Since this framework is very simple, the application of the following results to real cases may exhibit certain limitations. However, it can be beneficial for a better understanding of the advantages of the KFS method.

The 1D domain contains $N = 100$ points, which are uniformly distributed over a mesh with a spacing Δx. One wants to find the optimal location of a single targeted observation ($N_t = 1$), that measures the same quantity as the analysis variable. One assumes that the sensitivity field $\nabla_{\mathbf{x}} J$ has already been calculated, and this sensitivity field is simulated here using simple trigonometric functions. The sensitivity at point x_k is assumed to follow

$$g(x_k) = \beta_g \cos\{2\pi(x_k - x_g)/\lambda_g\} \exp(-|x_k - x_g|/L_g), \tag{25}$$

where x_g is the location of the maximum sensitivity, L_g is the characteristic length-scale of the sensitive area, λ_g is the frequency of oscillation of the gradient field inside the sensitive area and β_g is a constant amplitude factor. In the following experiment, the maximum amplitude of the gradient field is located in the middle of the domain

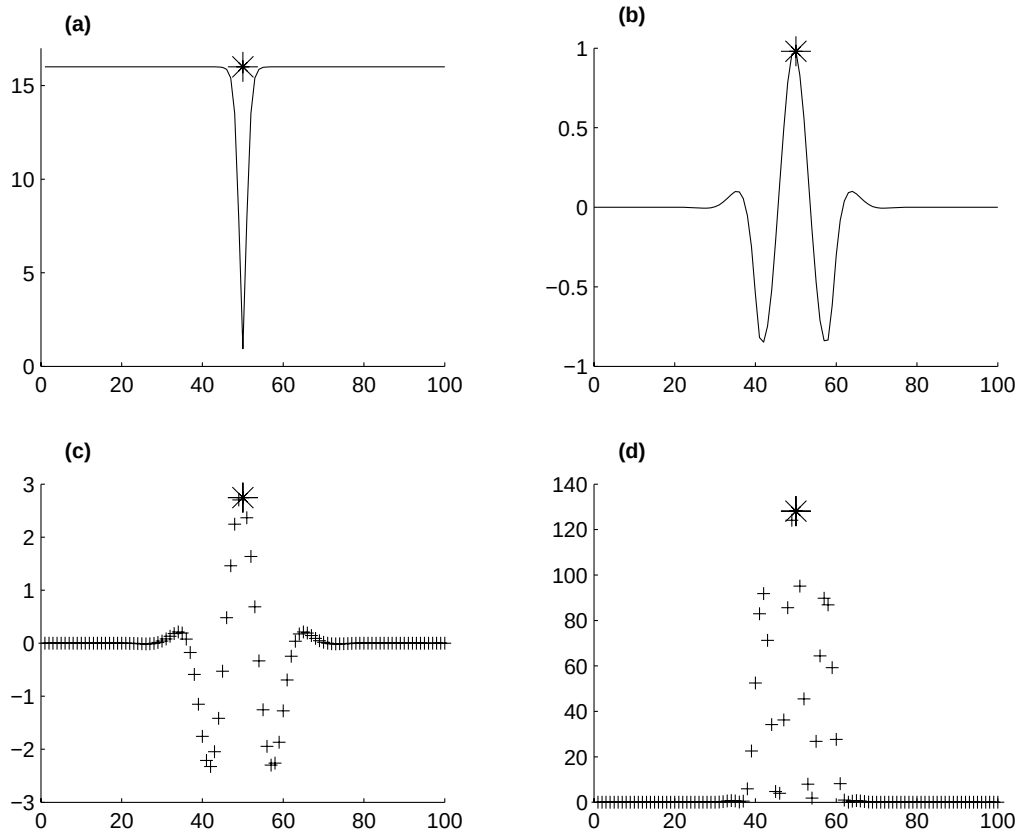

Figure 1. Experiment for an aspect ratio $L_b/L_g = 0.1$: (a) diagonal terms of the covariance analysis matrix A_{c+t}, (b) sensitivity to initial conditions $\nabla_{\mathbf{x}} J$, (c) sensitivity to targeted observation $\nabla_{\mathbf{y}_t} J$, and (d) reduction of the variance of the forecast error $(\delta\sigma_S^t)^2$. See text for explanation of symbols. In (c) and (d) the value of the sensitivity to observation and of the reduction of variance is plotted with a + for the different location of the single targeted observation. The large + sign corresponds to the optimal location for the sensitivity to observation method, while the large $*$ corresponds to the optimal location for the KFS method (as explained in the text, both optimal locations are the same for this particular case).

($X_g = 50\Delta x$), and the frequency of oscillation of the gradient field is taken as $\lambda_g = (3/2)L_g$. With this value of λ_g, the sensitivity field looks as in reality. Different tests have shown that the results presented hereafter are not affected by small changes of λ_g around this value. The gradient field tends towards zero over most of the domain, and is non-zero inside a limited area (called the sensitive area) of characteristic length-scale L_g (see Fig. 1(b)). It can be remarked that this framework is significantly different from the 1D study of Baker and Daley (2001), in the sense that only a fraction of the domain is sensitive to initial conditions. It can also be seen that this gradient field is symmetric with respect to X_g.

The background-error covariance $\mathbf{B}$ is an $N \times N$ matrix where element $b_{j,k}$ is given by a second-order autoregressive function

$$b_{j,k} = \sigma_b^2(1 + d(j,k)/L_b)\exp(-d(j,k)/L_b), \tag{26}$$

where L_b is the correlation length for the background error; $d(j,k)$ is the distance between points x_j and x_k and is given, in this simple case, by $d(j,k) = |j-k|\Delta x$; σ_b^2 is the background-error variance, and can be seen as a scaling factor. It is important

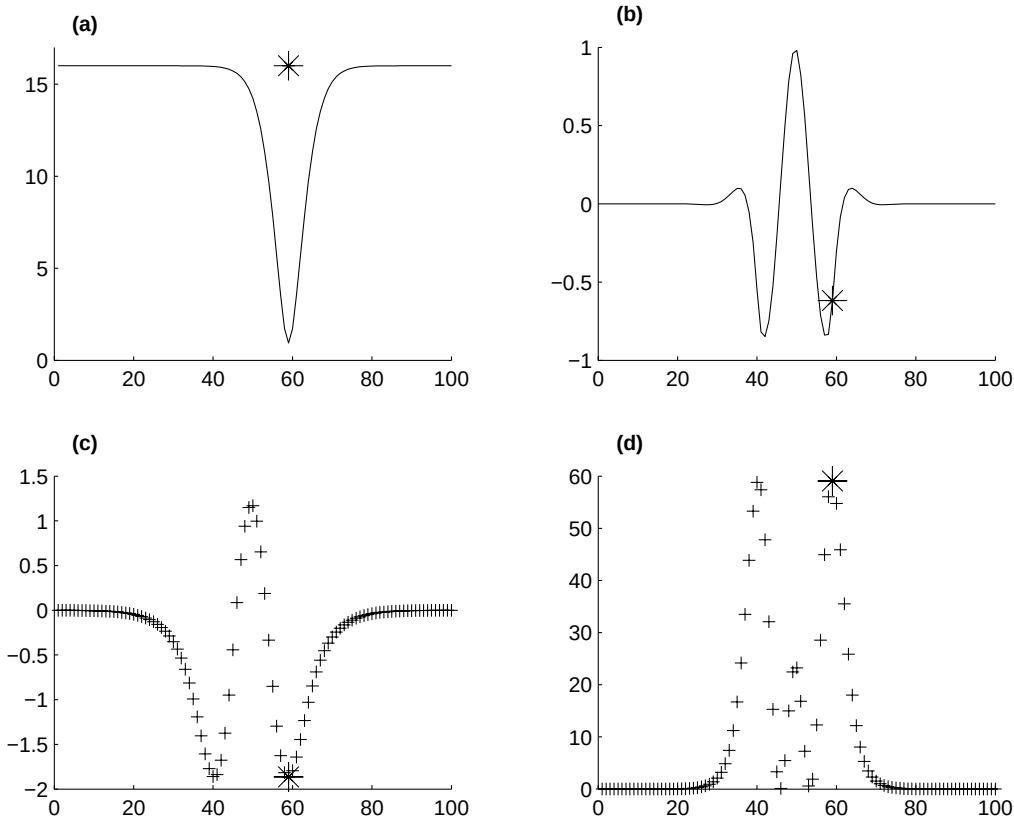

Figure 2. Same as Fig. 1 for an aspect ratio $L_b/L_g = 0.4$.

to note that this formulation of **B** assumes quasi-isotropic error correlations in the guess field. Therefore, the simple framework studied here is typical of a 3D-Var assimilation scheme. It should be noted that some of the conclusions might change if the data assimilation assumed flow-dependent error covariances, as for 4D-Var.

(*b*) *Case with constant analysis variance error*

The first simple targeting situation is the case where the variance of the conventional observations analysis-error matrix is homogeneous (i.e. the diagonal term of matrix $\mathbf{A}_c$ is homogeneous). This case can arise if there are no conventional observations inside, or close to, the sensitive area. In this case, the conventional-analysis error covariance matrix is equal to the background-error covariance matrix, $\mathbf{A}_c = \mathbf{B}$ inside the sensitive area. Following the simple 1D framework previously described, the variance term σ_a^2 (i.e. the diagonal term of matrix $\mathbf{A}_c$) is therefore constant and equal to σ_b^2. One assumes in this subsection that the conventional-analysis covariance is similar to Eq. (26). The accuracy of the measurement is set equal to $\sigma_o^2 = \sigma_b^2/16$.

As previously demonstrated under these hypotheses, the sensitivity to observations and the KFS method give the same optimal location of a single targeted observation (the maximum amplitude of $\mathbf{A}_c \cdot \nabla_{\mathbf{x}} J$). However, even in this very simple case, the optimal adaptive observation is not necessarily located where the sensitivity with respect to analysis, $\nabla_{\mathbf{x}} J$, is maximum, and it would be helpful to learn more about how

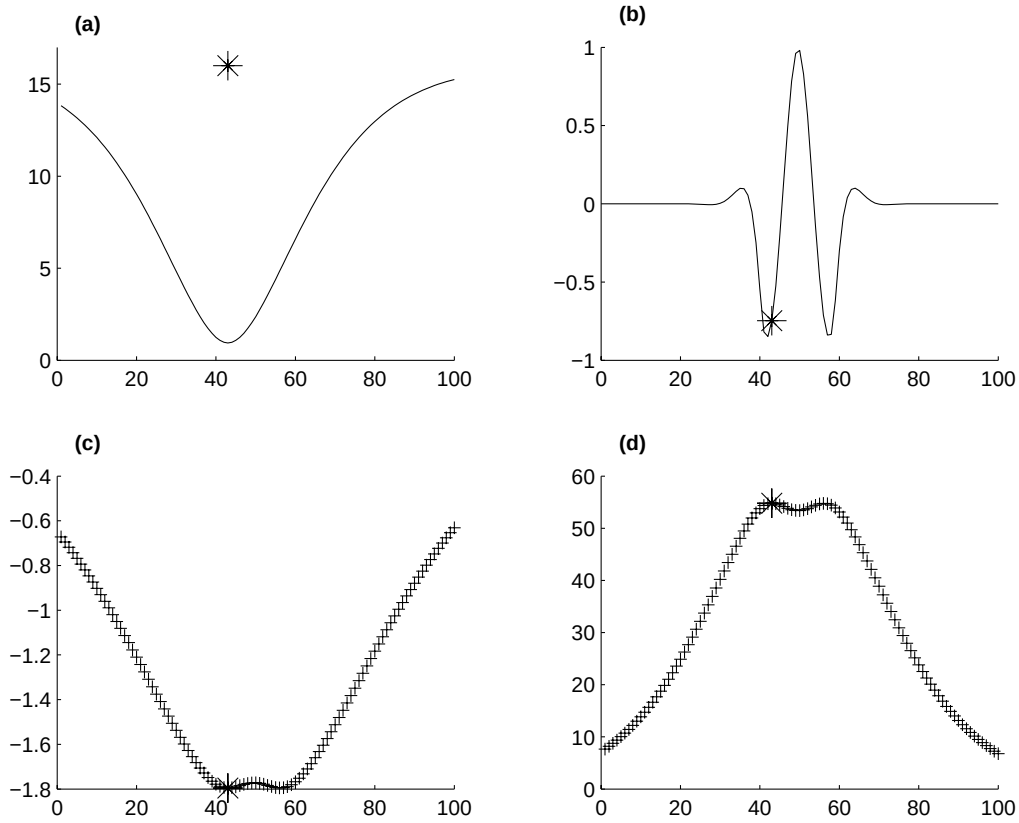

Figure 3. Same as Fig. 1 for an aspect ratio $L_b/L_g = 2.0$.

data assimilation schemes, and how instabilities in the model dynamics, will interact (as previously shown by Baker and Daley (2000)). The quantity $\delta\sigma_S^2$ (and also $\nabla_{\mathbf{y}} J$) depend on two length-scales: the gradient length-scale L_g, and the conventional-analysis correlation length-scale L_b.

When the characteristic length-scale of the conventional-analysis error correlation is much smaller than the characteristic length-scale of the sensitivity, i.e. $L_b \ll L_g$, Eq. (19) may be approximated by $(\delta\sigma_S^i)^2 = g(x_i)^2\sigma_a^4/(\sigma_a^2 + \sigma_o^2)$. Then, the optimal single targeted observation is located at the maximum of the absolute value of sensitivity with respect to analysis. An example of such a scenario is given in Fig. 1, for an aspect ratio $L_b/L_g = 0.1$. In such a case, all the useful information is contained in the dynamical instability, and therefore in the classical gradient field with respect to initial conditions.

If the characteristic length-scale of the gradient and of the conventional-analysis error correlation is roughly similar, interactions between the observations, the data assimilation system and the forecast model become more complex. Such an example is given in Fig. 2, for an aspect ratio $L_b/L_g = 0.4$. It can be noted that the optimal targeted observation is not located at the extremum of the gradient field. Moreover, an observation located at the maximum of the gradient (point 50) leads to a reduction of the forecast variance of about $1/3$ of the reduction due to the optimal observation. In such a case, all information present in both the gradient field and the conventional-analysis

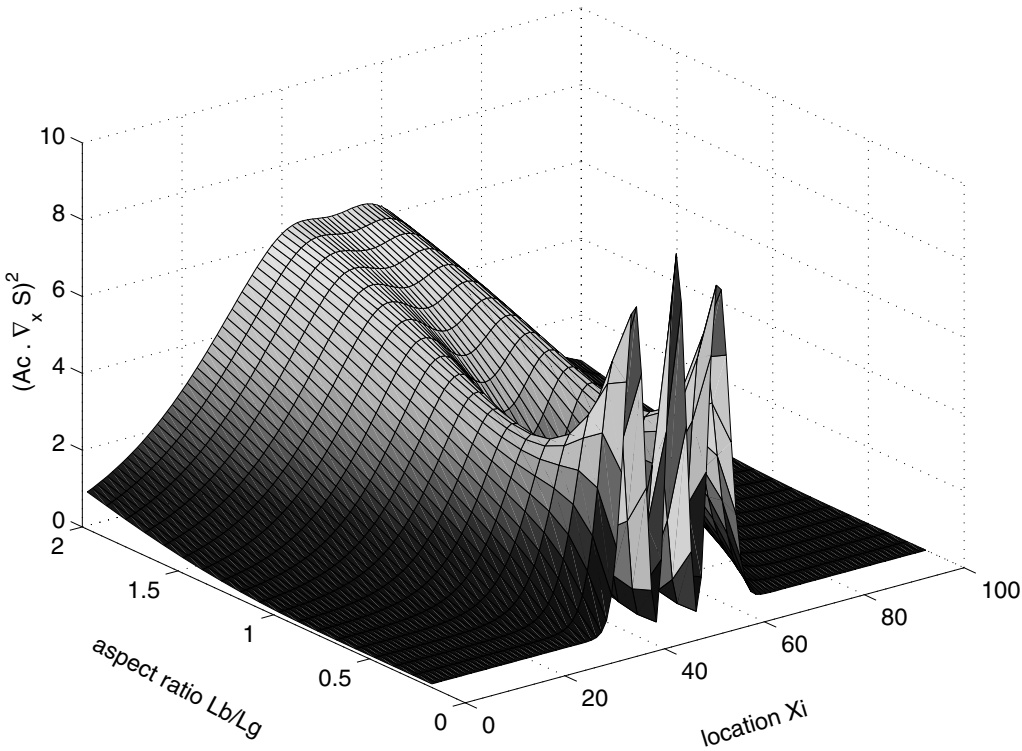

Figure 4. Variation of $\mathbf{A_c} \cdot \nabla_{\mathbf{x}} J$ as a function of the aspect ratio and location in the domain (see text for explanation).

error correlation is important, and should be taken into account to find the optimal location of the targeted observation. It can be seen that this result implies that a single targeted observation located in a region where the sensitivity is strong, but changes sign rapidly (with respect to the conventional-analysis error length-scale), leads to a very small impact on the forecast score. Conversely, a single targeted observation located in a region where the sensitivity is relatively small, but with few changes of sign, leads to a relatively large decrease of the forecast-score variance.

If $L_\mathrm{b}/L_g = 2$, it can be seen in Fig. 3 that any observation located inside the sensitive area has about the same impact, in terms of the reduction of the score variance (or in terms of sensitivity to observations). This behaviour can be explained by the wide influence of the observation: any observation located inside the sensitive area will modify the initial conditions in the same way. It can also be noted that the effect of the targeted observation is reduced by a factor of $1/2$ for sensitivity to observation (Figs. 1(c) and 3(c)) and for the reduction of variance (Figs. 1(d) and 3(d)). This proves that the efficiency of targeted observations also depends on the characteristics of the assimilation scheme, as previously demonstrated by Baker and Daley (2000), Bergot (2001) and Doerenbecher and Bergot (2001). This kind of experiment also allows discussion of the effects of wrong background-error covariance assumptions on the estimation of the reduction of the forecast-score variance. For example, one clearly sees that the effect of assuming a larger scale in background-error covariance would lead to an *underestimation* of the reduction of the forecast-error variance (cf. Figs. 1(d) and 3(d)) with the KFS method.

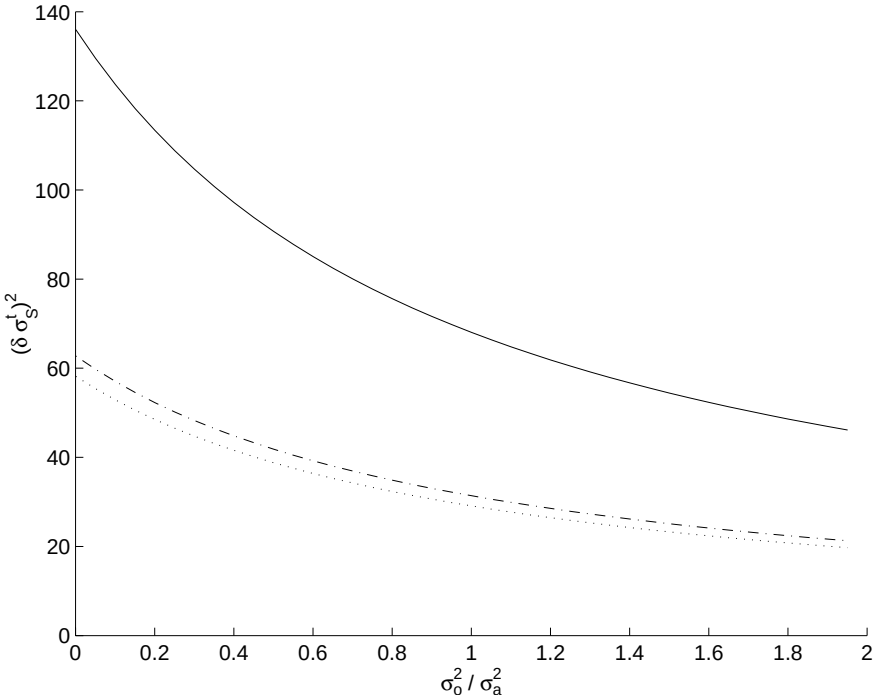

Figure 5. Variation of $(\delta\sigma_S^t)^2$ (see text) as a function of the accuracy of the measurement, for the three studied aspect ratios: $L_b/L_g = 0.1$ (solid line), $L_b/L_g = 0.4$ (dash-dotted), and $L_b/L_g = 2.0$ (dotted).

As previously explained, in the case of a single targeted observation and uniform σ_a^2, the optimal location is given by the maximum of $\mathbf{A}_c \cdot \nabla_{\mathbf{x}} J$. In Fig. 4, $(\mathbf{A}_c \cdot \nabla_{\mathbf{x}} J)^2$ is plotted as a function of both the aspect ratio L_b/L_g and the location x_i of the observation. Figure 4 allows the optimal location for different aspect ratios to be found easily. The behaviour of this efficiency is relatively complex. However, it is noteworthy that the area near the maximum of the gradient can correspond to a minimum in the efficiency for many aspect ratios. Even in this very simple case, not only the sensitivity field is important, but also the characteristic length-scale of the covariance errors which should be taken into account for finding the optimal location of targeted observations.

In the simple case studied, the optimal location of the targeted observations does not depend on the accuracy of the measurement σ_o^2. However, the estimation of the forecast-error variance depends on σ_o^2. Figure 5 displays the variation of variance reduction, $\delta\sigma_S^i$, at the optimal location as a function of σ_o^2, for the three aspect ratios that were previously studied. Following Eq. (24), the shape of the curves follows a function of the type $\alpha/(1+X)$ where $\alpha = \sigma_a^2 I^2(i)$ and $X = \sigma_o^2/\sigma_a^2$. The maximum reduction of the variance is α and is obtained for very accurate measurements. This limit depends on the aspect ratio L_b/L_g: the smaller the length-scale of the error correlation function assumed by the data assimilation scheme, the more efficient targeted observation is. This illustrates that the reduction of forecast-error variance would be higher when the length-scale of the correlations assumed in **B** are smaller.

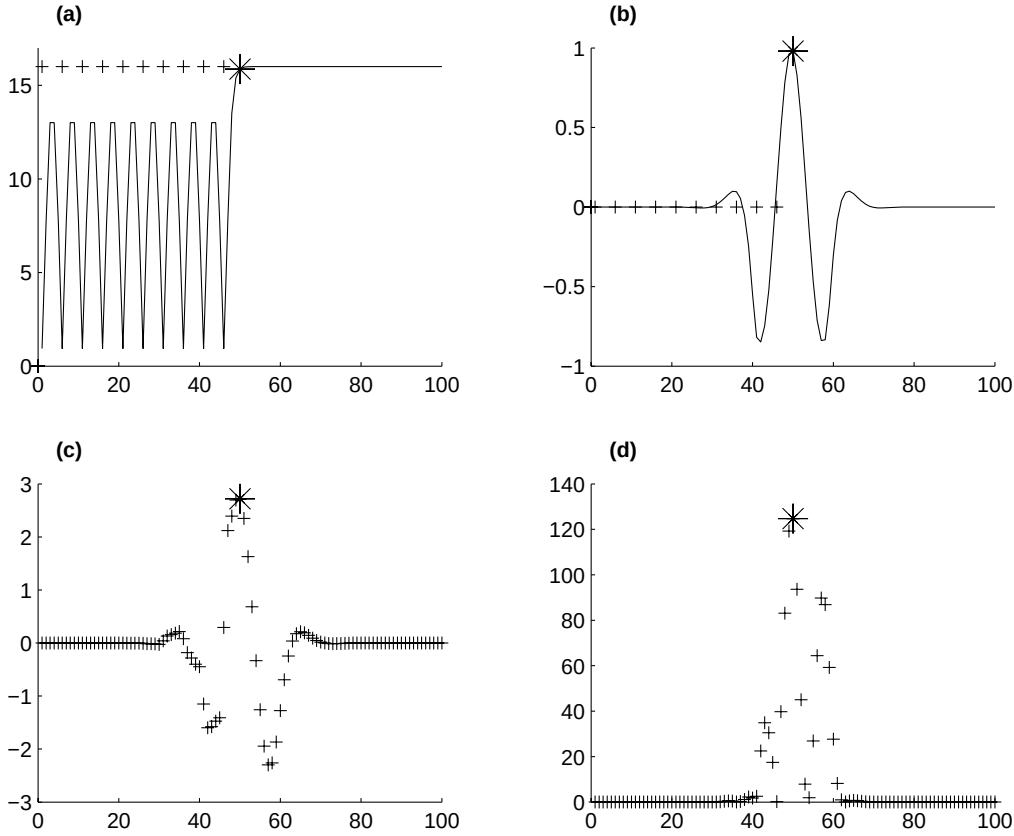

Figure 6. Same as Fig. 1 for the coastline case and an aspect ratio $L_b/L_g = 0.1$. The conventional observations are plotted with a + in (a) and (b). The large + corresponds to the optimal location for the sensitivity to observation method, while the large $*$ corresponds to the optimal location for the proposed method. Both optimal locations are the same for this aspect ratio.

(*c*) *Simulation of a coastline*

In this subsection, we simulate a situation in which the target region is located close to a coastline. This case frequently occurred during FASTEX, and it was then difficult to define a flight plan since the influence of conventional observations on the sampling of the sensitivity area was unknown. One assumes here that there is a conventional observation every 5th grid point over the so-called 'land' while there are no conventional observations over the so-called 'ocean'. This distribution is consistent with the classical distribution of radio-sounding over North America and the North Atlantic Ocean. The background term **B** is expressed as in Eq. (26). As previously done, three different aspect ratios $L_b/L_g = 2$, 0.4 and 0.1 are studied. The accuracy of both conventional and targeted observations are equal to $\sigma_o^2 = \sigma_b^2/16$, as in section 4(b). The location of targeted observations are tested over land and ocean, indiscriminately.

Figure 6 shows the case where $L_b/L_g = 0.1$. In such a case, the three methods (sensitivity with respect to initial condition, sensitivity with respect to targeted observation, and the simplified KFS), give the same location for the optimal single targeted observation. This optimal targeted observation is located where the sensitivity with respect to initial conditions is maximum.

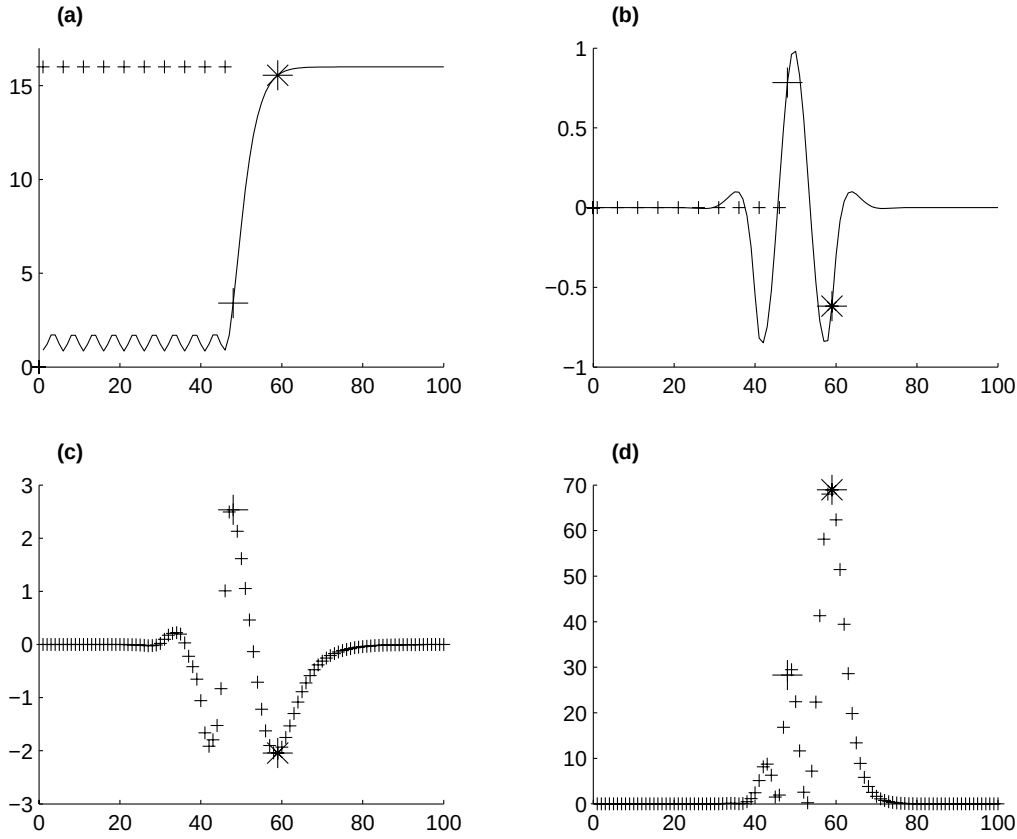

Figure 7. Same as Fig. 6 for an aspect ratio $L_b/L_g = 0.4$.

If the characteristic length-scale of the gradient and of the conventional analysis-error correlation are roughly similar, the three methods give relatively different results (Fig. 7). As noted by Baker and Daley (2000), one observes a phenomenon of super-sensitivity to observation at the border between ocean and land. A comparison of Figs. 2(c) and 7(c), shows that the sensitivity with respect to observation is multiplied by a factor 2 near the coastline, and the optimal targeted observation from the sensitivity to observation method is clearly located at the coastline, as previously shown by Baker and Daley (2000). The KFS method gives significantly different results, consistent with the explanation given in section 3(b). In fact, this method also takes into account the structure and amplitude of the errors in the conventional analysis fields, and consequently the optimal targeted observation is clearly located over the ocean. An increase in the maximum reduction of the forecast-error variance can be noted (Figs. 2(d) and 7(d)). This phenomenon can be seen as a super-sensitivity, as previously. This is a consequence of the conventional data located at the border of the sensitive area.

And finally, if $L_b/L_g = 2$, it can be seen in Fig. 8 that the three methods also lead to different results. However, the three optimal locations are closer than in the previous case (three points between the sensitivity to observation and the KFS). Another important point is that, in such a case, the reduction of the variance of the forecast score

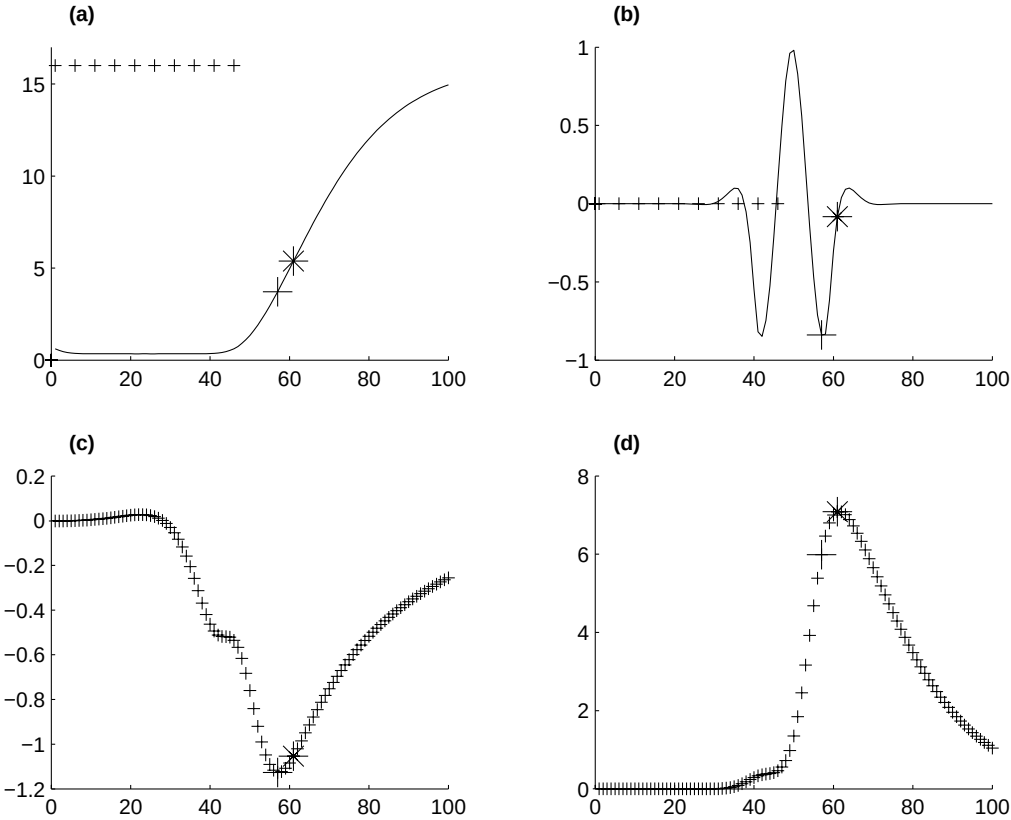

Figure 8. Same as Fig. 6 for an aspect ratio $L_\mathrm{b}/L_g = 2.0$.

is about $1/8$ of the homogeneous case (Figs. 3(d) and 8(d)). A reduction is also observed for the sensitivity to observations, but with a factor $3/2$.

In conclusion, one can remark that the aspect ratio L_b/L_g, and thus the optimal sampling, depends on numerous parameters. In fact, the length-scale L_b varies as a function of the measured parameters, the vertical level, and the geographical and meteorological situations. The length-scale L_g also varies as a function of the model parameters, model levels, meteorological situations and forecast aspect J. Consequently, it is not trivial to define a universal aspect ratio L_b/L_g valid for real numerical weather-forecast models. The results presented here certainly depend on the behaviour of the gradient field, and the simple framework used here may limit their validity in the context of a real numerical weather-forecast models. However, these findings illustrate very well the non-trivial nature of optimal sampling in a sensitive area. Moreover, since forecast errors grow nonlinearly and since error covariances in the operational assimilation scheme are not accurately specified, the KFS method could lead to errors in the definition of the optimal sampling. While these results in a simple context seem encouraging, it is necessary to evaluate the robustness of the KFS method in an operational numerical weather-prediction context.

5. Application in an operational context

(*a*) *Context*

The previous sections have focused on applications of the KFS method in a simplified context. In the future, it is envisioned that this method will be used in an operational context to examine different sampling strategies. For example, we hope to use this method during the future THORPEX experiment*. However, the KFS results might also be used in a diagnostic way (once the observations are made) in order to understand results obtained during previous field experiments, such as FASTEX, January to February 1997†. This is the main aim of this section.

The focus here is on four FASTEX Intensive Observing Period (IOP) flights for which soundings collected by the Gulfstream IV are available (see Bergot (2001) for more details): IOP15, IOP17 (2 flights) and IOP18. These flights have been studied in detail by different teams (see, for example, Langland *et al.* 1999b; Gelaro *et al.* 1999; Cammas *et al.* 1999; Bergot 1999).

The model used is the French Arpege/Integrated Forecast System operational model, developed in collaboration with the European Center for Medium-Range Weather Forecasts (Courtier *et al.* 1991). The assimilation scheme is an incremental 3D-Var, and the covariance analysis-error matrix is estimated following the work by Fisher and Courtier (1995) and Doerenbecher and Bergot (2001). The conventional observations used in this application are similar to those used for studying the efficiency of FASTEX targeted observations (Bergot 1999, 2001). The forecast aspect J is the enstrophy, integrated vertically around 850 hPa, over the horizontal verification area (35°N–65°N, 30°W–0°). This score is the same as the one used during the FASTEX field experiment.

(*b*) *Validation in diagnostic mode*

A previous study has enabled us to estimate the improvement of the forecasts, resulting from the inclusion of targeted data, in a systematic way (Bergot 2001). A summary of the improvement of the forecasted kinetic energy for the four cases studied is given in Table 1 (see Bergot (2001) for more details). It can clearly be seen that two flights strongly improve the forecast: the first flight for IOP17 and the flight for IOP18. For the four flights studied, the data assimilation scheme's estimate of the variance of the forecast error has been computed for different scenarios (Fig. 9): without data, $(\nabla_{\mathbf{x}} J)^{\mathrm{T}} \cdot \mathbf{B} \cdot \nabla_{\mathbf{x}} J$; with conventional data only, $(\nabla_{\mathbf{x}} J)^{\mathrm{T}} \cdot \mathbf{A}_{\mathrm{c}} \cdot \nabla_{\mathbf{x}} J$; with targeted data only, $(\nabla_{\mathbf{x}} J)^{\mathrm{T}} \cdot \mathbf{A}_{\mathrm{t}} \cdot \nabla_{\mathbf{x}} J$; and with targeted data added to conventional ones, $(\nabla_{\mathbf{x}} J)^{\mathrm{T}} \cdot \mathbf{A}_{\mathrm{c+t}} \cdot \nabla_{\mathbf{x}} J$.

One case (IOP15, 15 February 1997) corresponds to a very small variance of the forecast error in the direction of the sensitivity (about $1/36$ of that from the first flight for IOP17), even without data. The inclusion of the conventional data further decreases this variance. Even without targeted data, the forecast for this IOP15 exhibits a strong confidence. The KFS method applied to these data gives the smallest reduction of the variance of forecast score and implies that this flight is inefficient. This result is in agreement with the result from the systematic study of the influence of FASTEX targeted data.

The second flight for IOP17 (18 February 1997) has a stronger variance of the forecast score arising from the background field. However, the inclusion of the conventional

* The Hemispheric Observing Research Program Experiment, see http://www.nrlmry.navy.mil/~langland/THORPEX_document/THORPEX_plan.pdf for details.

† See http://www.cnrm.meteo.fr/fastex/

TABLE 1. IMPROVEMENT OF THE FORECAST KINETIC ENERGY DUE TO THE INCLUSION OF TARGETED DATA FOR THE FOUR CASES STUDIED

IOP	Initial time	Final time	Duration	Improvement (J kg^{-1})
IOP15	06 UTC 15 February	00 UTC 16 February	18 h	42.68
IOP17	18 UTC 17 February	12 UTC 19 February	42 h	329.39
IOP17	18 UTC 18 February	12 UTC 19 February	18 h	37.26
IOP18	12 UTC 22 February	12 UTC 23 February	24 h	147.47

All dates are 1997. See Fig. 8 of Bergot (2001) for more detail.

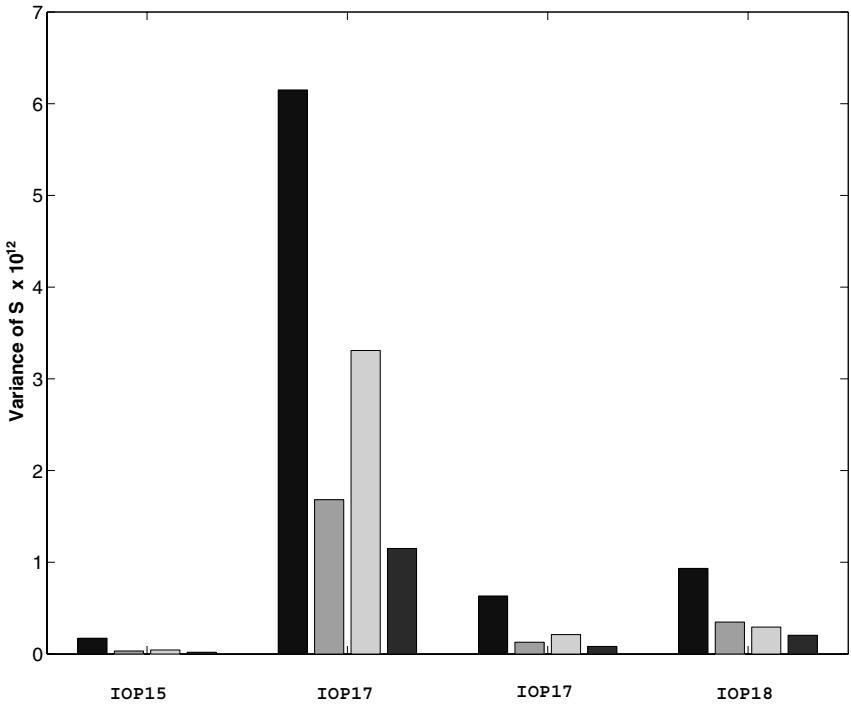

Figure 9. The variance of the forecast score for the four studied cases. Left to right bars: without data, $(\nabla_{\mathbf{x}} J)^{\mathrm{T}} \cdot \mathbf{B} \cdot \nabla_{\mathbf{x}} J$; with conventional data only, $(\nabla_{\mathbf{x}} J)^{\mathrm{T}} \cdot \mathbf{A}_{\mathrm{c}} \cdot \nabla_{\mathbf{x}} J$; with targeted data only, $(\nabla_{\mathbf{x}} J)^{\mathrm{T}} \cdot \mathbf{A}_{\mathrm{t}} \cdot \nabla_{\mathbf{x}} J$; and with targeted data added to conventional ones, $(\nabla_{\mathbf{x}} J)^{\mathrm{T}} \cdot \mathbf{A}_{\mathrm{c+t}} \cdot \nabla_{\mathbf{x}} J$. See Table 1 for times of IOPs and text for further explanation.

data strongly decreases this variance (by about 80%), and the effect of the targeted data, given the conventional network of observations, is relatively weak. Again, this flight is relatively inefficient, and this result is in agreement with Table 1.

The first flight for IOP17 (17 February 1997) is noteworthy in the sense that the error variance of the forecast resulting from the background field is the highest of the four studied cases. However, as for the second flight for this IOP (18 February 1997), the conventional data strongly reduce this variance (by about 74%). The positive effect of the targeted data added to conventional ones on the variance of the score clearly appears, and represents a reduction of about 31% of the variance of the forecast resulting from the analysis based on conventional observations only.

However, the more interesting case is IOP18 (22 February 1997). For this case, the effect of the targeted observations on the variance of the score is higher than the effect

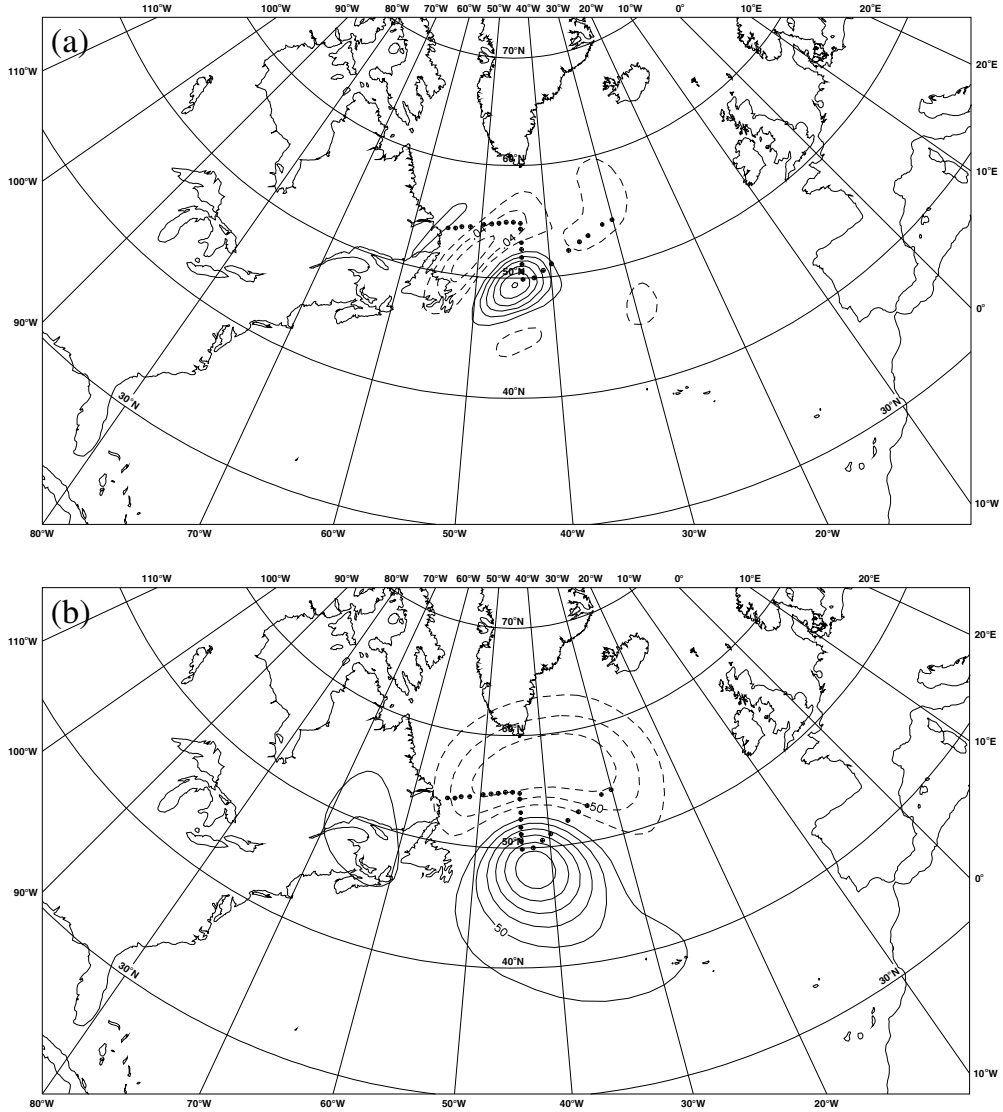

Figure 10. IOP18 (22 Feb 1997): (a) the sensitivity field for temperature at model level 23 (about 800 hPa), and (b) the product of the sensitivity field and the conventional-analysis error variance, $\mathbf{A}_{\mathbf{c}} \cdot \nabla_{\mathbf{x}} J$ (see text). The black dots are the flight path.

of the conventional ones, even though only 25 dropsondes are available. The inclusion of the targeted observations leads to a reduction of the forecast-score variance by about 42%. Other studies performed with different assimilation schemes and models (Langland *et al.* 1999b; Bergot 2001) have previously demonstrated that this case is a success from the targeting point of view. The KFS result is in agreement with these studies.

(*c*) *Towards an application in a prognostic mode*

In order to understand the optimal deployment of observations given by KFS, Figs. 10(a) and (b) show the classical sensitivity field and the product $\mathbf{A}_{\mathrm{C}} \cdot \nabla_{\mathbf{x}} J$, respectively, for FASTEX IOP18. As previously mentioned, the targeted observations

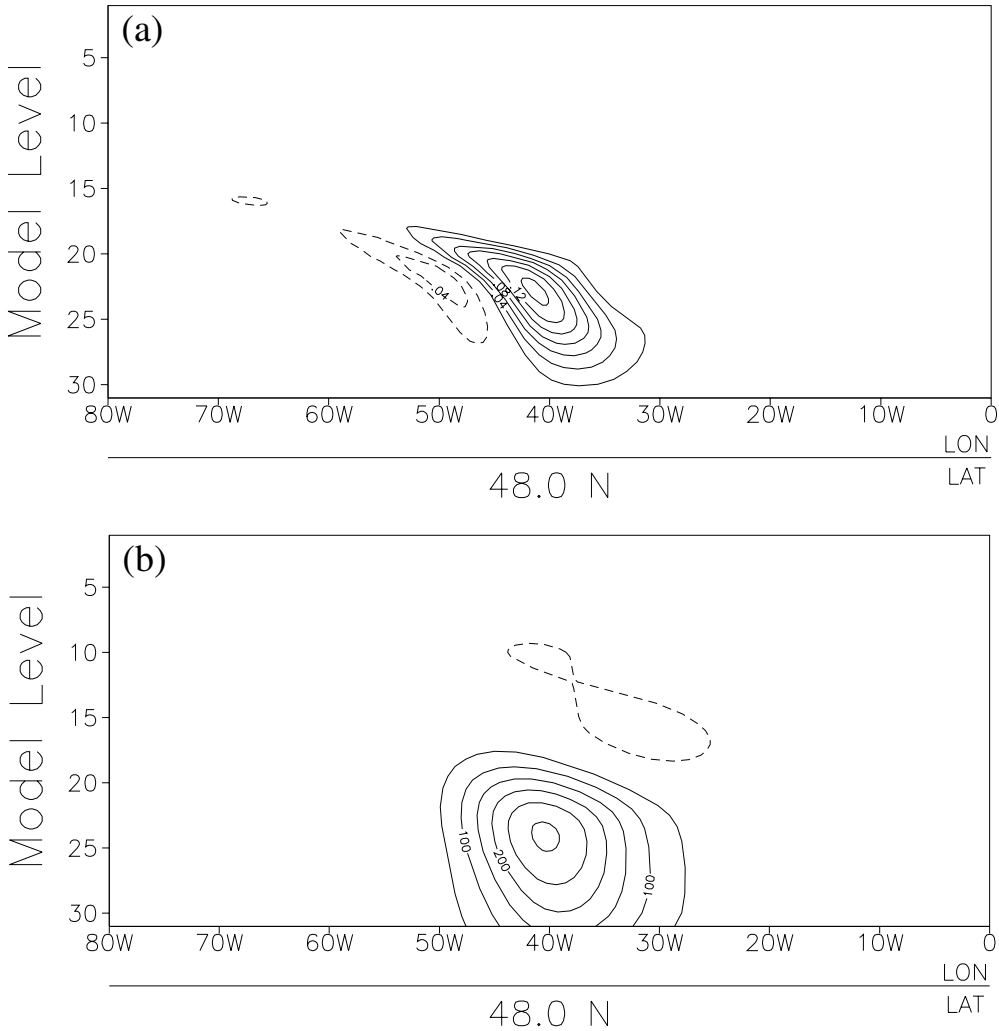

Figure 11. Vertical cross-section along 48°N for the same fields as in Fig. 10.

performed during this case are very efficient. The product $\mathbf{A}_C \cdot \nabla_{\mathbf{x}} J$ corresponds to the first term of the KFS method (Eq. (15)). As previously explained, if the length-scale of the analysis-error covariance matrix is large with respect to the length-scale of the sensitivity field (at least over the ocean), the KFS method can be summarized by this product. First it can be pointed out that the sensitive area defined with $\mathbf{A}_C \cdot \nabla_{\mathbf{x}} J$ (Fig. 10(b)) extends further horizontally than the sensitive area defined with the classical sensitivity field (Fig. 10(a)). The second point concerns the vertical structure of the sensitive area. Figure 11(a) shows a vertical cross-section of the classical sensitive area, and one can see the typical very pronounced vertical tilt. Figure 11(b) shows the same cross-section for $\mathbf{A}_C \cdot \nabla_{\mathbf{x}} J$. Clearly noticeable is a more barotropic structure, with only a smaller vertical tilt. However, the maximum of sensitivity is located at the lower levels for both sensitive areas (around model level 22, i.e. about 750 hPa). These results are

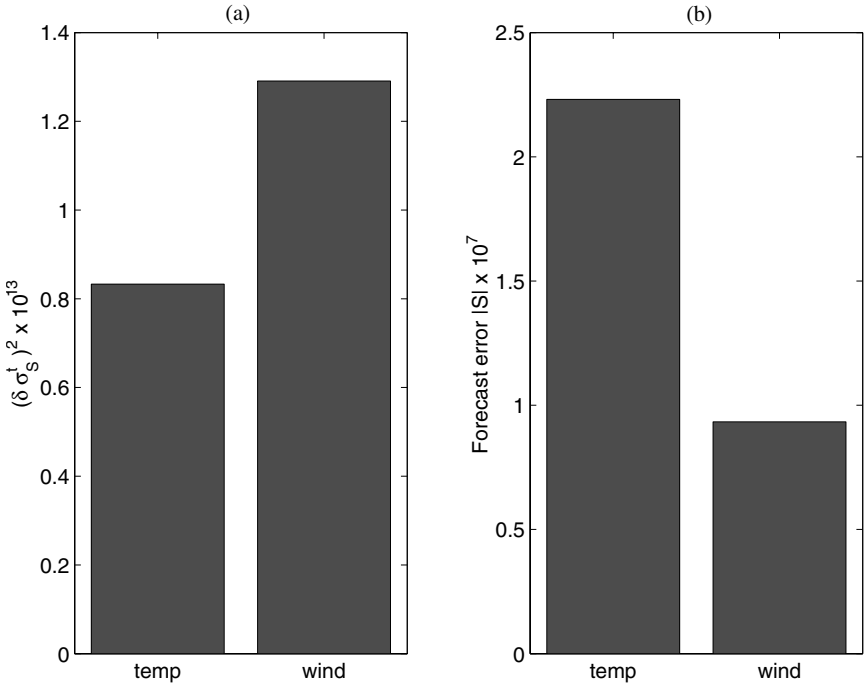

Figure 12. (a) Reduction of the forecast-error variance given by the KFS method, and (b) forecast error, for the experiment where targeted observations are only temperature measurements ('temp') or only wind measurements ('wind').

robust for the four studied cases, and are undoubtedly a consequence of the assimilation scheme used (3D-Var for this study).

The results of the previous section suggest that the KFS method can discriminate the cases where adaptive observations are needed and are efficient. However, this method must also be useful for making a choice between different possible deployments of observations. To illustrate this point, the flight for IOP18 has been decomposed into two deployments: in the first one, only temperature measurements from dropsondes are taken into account (experiment called 'temp'), and in the second one assumes that only wind measurements have been performed (experiment called 'wind'). Figure 12 shows the reduction of the forecast-error variance given by KFS, $(\delta\sigma_S^t)^2$, and the forecast error $|S| = |J(\mathbf{X}) - J(\mathbf{X}_{\text{true}})|$, where $\mathbf{X}_{\text{true}}$ is given by the analysed value. Note that the 'wind' deployment of observations leads to a significantly stronger reduction of forecast-error variance than in the 'temp' one (Fig. 12(a)). Associated with this decrease in the forecast-error variance, Fig. 12(b) shows a significant decrease of the forecast error for the 'wind' experiment. For this particular case, the efficiency of targeted observations is clearly a consequence of the wind measurements, and this result is in agreement with the result given by the KFS method. This preliminary result allows us to be optimistic. However, it will be necessary to validate the KFS method for numerous cases.

6. Conclusion

A new technique, called Kalman Filter Sensitivity (KFS), has been proposed for identifying the optimal deployment of an adaptive observation network. The KFS

method allows the quantification of how targeted observations would reduce the variance of a given forecast score (such as enstrophy or kinetic energy, inside a verifying area for example). This estimation is consistent with the statistics used during the assimilation, and with the dynamics of the atmosphere, given by a classical sensitivity field.

A very simple application of this technique in a 1D problem has been performed. This framework allows a 3D-Var assimilation scheme to be simulated. These preliminary results show that the sampling of a sensitive area is strongly constrained by the aspect ratio between the length-scale of the sensitivity area and of the conventional analysis-error covariance matrix. If the sensitivity varies little with respect to conventional-analysis covariance, all the useful information is summarized by the classical gradient field. In other cases, it is not trivial to find the optimal location of targeted observations, and the assimilation scheme, the sensitivity field and the analysis covariance errors associated with conventional observations, should be all taken into account. For example, an observation located in a region where the sensitivity is strong, but changes sign rapidly, leads to a very small reduction of the forecast-error variance of the chosen forecast aspect. In this case, the more efficient observations can be located at the border of the sensitivity field or near a coastline (region of super-sensitivity as previously mentioned by Baker and Daley (2000)). This work also clearly demonstrates that the sampling of the sensitive area strongly depends on the covariance of the analysis errors. A definition of an optimal deployment of targeted observations (in the sense of a minimum number of observations for a maximum improvement of the forecast) should therefore include the characteristics of the statistics of these errors.

An advantage of the KFS method compared to other adjoint-based targeting techniques is that it provides an explicit technique for computing the reduction of the variance of the forecast of a given score as a function of different deployments of observations. This is only strictly true if the observation- and background-error covariance are accurately specified, and if the errors evolve linearly. In order to test the validity of this computation, the KFS technique has been employed in a diagnostic way on four FASTEX cases. For the four studied cases, the reduction of the variance of the forecast score given by the KFS method is in agreement with the systematic survey of the efficiency of FASTEX flights (Bergot 2001). In the two cases of small improvement of the forecast (IOP15 and second flight for IOP17), the KFS technique indicates a small reduction of the forecast-error variance. Against this, in the two cases of strong improvement of the forecast (first flight for IOP17 and IOP18), the KFS method suggests a strong reduction of the forecast-error variance. The IOP18 is noteworthy in the sense that the reduction of the forecast-error variance due to the targeted observations alone (25 dropsondes, without conventional observations) is stronger than the reduction of the forecast-error variance due to conventional observations. For this IOP18, two complementary deployments of targeted observations have been studied: the first one only contains temperature measurements, and the second only wind measurements. For these cases, the wind measurements are the most efficient in the sense of the forecast score imposed (enstrophy). The KFS method is in total agreement with this result: the assimilation of wind measurements will lead to a stronger reduction of forecast variance.

These results seem to validate the KFS approach for targeting purposes. It is important now to study the use of this tool in a prognostic mode (before the conventional and targeted observations are done), in order to try to optimize a network of targeted observations. What will be the most efficient deployment of targeted observations, given the conventional network of observations, the assimilation scheme and the actual instabilities of the atmosphere? To answer this kind of question, it is now necessary to test the KFS method for numerous cases. This can be achieved for example in numerical

simulations, such as the Observing System Simulation Experiment, and during field experiments, such as the future THORPEX experiment. This kind of experiment will allow the strengths and weaknesses of KFS to be evaluated.

ACKNOWLEDGEMENTS

We are particularly grateful to Philippe Lopez, Gérald Desroziers and Florence Rabier for helpful comments on the first version of this article. The authors also address special thanks to Mike Fisher for his friendly help concerning the estimation of the analysis-error covariance matrix. Our colleagues from the Centre National de Recherches Météorologiques/Groupe de Modelisation à Meso-Echelle team are also strongly acknowledged for their daily scientific and technical support. And finally, we would also like to thank the anonymous referees for their relevant comments and criticisms.

REFERENCES

Baker, N. L.	2000	'Observation adjoint sensitivity and the adaptive observation-targeting problem'. PhD thesis, Naval Postgraduate School, USA
Baker, N. L. and Daley, R.	2000	Observation and background adjoint sensitivity in the adaptive observation targeting problem. *Q. J. R. Meteorol. Soc.*, **125,** 1431–1454
Bergot, T.	1999	Adaptive observations during FASTEX: A systematic survey of upstream flights. *Q. J. R. Meteorol. Soc.*, **125,** 3271–3298
	2001	Influence of the assimilation scheme on the efficiency of adaptive observations. *Q. J. R. Meteorol. Soc.*, **127,** 635–661
Bergot, T., Hello, G., Joly, A. and Malardel, S.	1999	Adaptive observations: a feasibility study. *Mon. Weather Rev.*, **127,** 743–765
Berliner, L. M., Lu, Z. Q. and Snyder, C.	1999	Statistical design for adaptive weather observations. *J. Atmos. Sci.*, **56,** 2536–2552
Bishop, C. H. and Toth, Z.	1999	Ensemble transformation and adaptive observations. *J. Atmos. Sci.*, **56,** 1748–1765
Bishop, C. H., Etherton, B. J. and Majumdar, S. J.	2001	Adaptive sampling with the ensemble transform Kalman filter. Part I: Theoretical aspects *Mon. Weather Rev.*, **129,** 420–436
Cammas, J. P., Pouponneau, B., Desroziers, G., Santurette, P., Joly, A., Arbogast, P., Mallet, I., Caniaux, G. and Mascart, P.	1999	FASTEX IOP17 cylone: Introductory synoptic study with field data. *Q. J. R. Meteorol. Soc.*, **125,** 3393–3414
Courtier, Ph., Freydier, C., Geleyn, J. F., Rabier, F. and Rochas, M.	1991	'The ARPEGE project at Météo-France'. Pp. 193–231 in Proceedings of ECMWF workshop on numerical methods in atmospheric models, 9–13 September 1991. European Centre for Medium-Range Weather Forecasts, Reading, UK
Doerenbecher, A. and Bergot, T.	2001	Sensitivity to observations applied to FASTEX cases. *Nonlinear Processes in Geophysics*, **8,** 467–481
Emanuel, K. A. and Langland, R. H.	1998	FASTEX adaptive observation workshop. *Bull. Am. Meteorol. Soc.*, **79,** 1915–1919
Errico, R.	1997	What is an adjoint model? *Bull. Am. Meteorol. Soc.*, **78,** 2577–2591
Fedorov, V. V., Studden, W. J. and Klimko, E. M.	1972	*Theory of optimal experiment.* Academic Press, New York
Fisher, M. and Courtier, P.	1995	Estimating the covariance matrices of analysis and forecast error in variational data assimilation. ECMWF Tech. Memo No. 220. European Centre for Medium-Range Weather Forecasts, Reading, UK
Gelaro, R., Langland, R. H., Rohaly, G. D. and Rosmond, T. E.	1999	An assessment of the singular vector approach to targeted observing using the FASTEX dataset. *Q. J. R. Meteorol. Soc.*, **125,** 3299–3328
Harrison, M. S. J., Palmer, T., Richardson, D. S. and Buizza, R.	1999	Analysis and model dependencies in medium-range ensembles: Two transplant case-studies. *Q. J. R. Meteorol. Soc.*, **125,** 2487–2515

Joly, A., Browning, K. A., Bessemoulin, P., Cammas, J. P., Caniaux, G., Chalon, J. P., Clough, S. A., Dirks, R., Emanuel, K. A., Eymard, L., Lalaurette, F., Gall, R., Hewson, T. D., Hildebrand, P. H., Jorgensen, D., Langland, R. H., Lemaitre, Y., Mascart, P., Moore, J. A., Persson, P. O. G., Roux, F., Shapiro, M. A., Snyder, C., Toth, Z. and Wakimoto, R. M. 1999 Overview of the field phase of the Fronts and Atlantic Storm Track Experiment (FASTEX) project. *Q. J. R. Meteorol. Soc.*, **125,** 3131–3164

Langland, R. H., Toth, Z., Gelaro, R., Szynyogh, I., Shapiro, M. A., Majumdar, S. J., Morss, R., Rohaly, G. D., Velden, C., Bonds, N. and Bishop, C. H. 1999a The North Pacific Experiment (Norpex-98): Targeted observations for improved North American Weather Forecasts. *Bull. Am. Meteorol. Soc.*, **80,** 1363–1384

Langland, R. H., Gelaro, R., Rohaly, G. D. and Shapiro, M. A. 1999b Targeted observations in FASTEX: Adjoint-based targeting procedures and data impact experiments in IOPs 17 and 18. *Q. J. R. Meteorol. Soc.*, **125,** 3241–3270

Lorenz E. N. and Emanuel, K. A. 1998 Optimal sites for supplementary observation: Simulation with a small model. *J. Atmos. Sci.*, **55,** 399–414

Majumdar, S. J., Bishop, C. H., Etherton, B. J., Szunyoght, I. and Toth, Z. 2001 Can an ensemble transform Kalman filter predict the reduction in forecast-error variance produced by targeted observations? *Q. J. R. Meteorol. Soc.*, **127,** 2803–2820

Morss, R. E. 1999 'Adaptive observations: Idealized sampling strategies for improving numerical weather prediction'. PhD thesis, Massachusetts Institute of Technology, USA

Morss, R. E., Emanuel, K. A. and Snyder, C. 2001 Idealized adaptive observation strategies for improving numerical weather prediction. *J. Atmos. Sci.*, **58,** 210–234

Palmer, T. N., Gelaro, R., Barkmeijer, J. and Buizza, R. 1998 Singular vectors metrics and adaptive observations. *J. Atmos. Sci.*, **55,** 633–653

Rabier, F., Klinker, E., Courtier, P. and Hollingsworth, A. 1996 Sensitivity of forecast errors to initial conditions. *Q. J. R. Meteorol. Soc.*, **122,** 121–150

Szunyogh, I., Toth, Z., Morss, R., Majumdar, S., Etherton, B. J. and Bishop, C. H. 2000 The effect of targeted dropsonde observations during the 1999 Winter Storm Reconnaissance Program. *Mon. Weather Rev.*, **128,** 3520–3537